


ORIGINAL ARTICLE

Open Access



# Geometric Accuracy and Energy Absorption Characteristics of 3D Printed Continuous Ramie Fiber Reinforced Thin-Walled Composite Structures

Kui Wang<sup>1</sup>, Hao Lin<sup>1</sup>, Antoine Le Duigou<sup>2</sup>, Ruijun Cai<sup>1</sup>, Yangyu Huang<sup>1</sup>, Ping Cheng<sup>1,3</sup>, Honghao Zhang<sup>4\*</sup>  and Yong Peng<sup>1</sup>

## Abstract

The application of continuous natural fibers as reinforcement in composite thin-walled structures offers a feasible approach to achieve light weight and high strength while remaining environmentally friendly. In addition, additive manufacturing technology provides a favorable process foundation for its realization. In this study, the printability and energy absorption properties of 3D printed continuous fiber reinforced thin-walled structures with different configurations were investigated. The results suggested that a low printing speed and a proper layer thickness would mitigate the printing defects within the structures. The printing geometry accuracy of the structures could be further improved by rounding the sharp corners with appropriate radii. This study successfully fabricated structures with various configurations characterized by high geometric accuracy through printing parameters optimization and path smoothing. Moreover, the compressive property and energy absorption characteristics of the structures under quasi-static axial compression were evaluated and compared. It was found that all studied thin-walled structures exhibited progressive folding deformation patterns during compression. In particular, energy absorption process was achieved through the combined damage modes of plastic deformation, fiber pullout and delamination. Furthermore, the comparison results showed that the hexagonal structure exhibited the best energy absorption performance. The study revealed the structure-mechanical property relationship of 3D printed continuous fiber reinforced composite thin-walled structures through the analysis of multiscale failure characteristics and load response, which is valuable for broadening their applications.

**Keywords** Additive manufacturing, Continuous fiber, Biocomposite, Thin-walled structure, Geometric accuracy, Energy absorption

\*Correspondence:

Honghao Zhang  
[honghao\\_zhang@sdu.edu.cn](mailto:honghao_zhang@sdu.edu.cn)

Full list of author information is available at the end of the article



© The Author(s) 2023. **Open Access** This article is licensed under a Creative Commons Attribution 4.0 International License, which permits use, sharing, adaptation, distribution and reproduction in any medium or format, as long as you give appropriate credit to the original author(s) and the source, provide a link to the Creative Commons licence, and indicate if changes were made. The images or other third party material in this article are included in the article's Creative Commons licence, unless indicated otherwise in a credit line to the material. If material is not included in the article's Creative Commons licence and your intended use is not permitted by statutory regulation or exceeds the permitted use, you will need to obtain permission directly from the copyright holder. To view a copy of this licence, visit <http://creativecommons.org/licenses/by/4.0/>.

## 1 Introduction

The fiber reinforced plastic composite materials are extensively used in automotive and aerospace applications due to their advantages of high specific strength, high specific stiffness and designability [1–3]. In particular, researchers focused on improving the crashworthiness of thin-walled parts of vehicles by using composites as collapsible energy absorbers [4, 5]. The combination of materials and manufacturing processes had to be suitable to guarantee the safety of lives and properties during catastrophic crashes [6, 7]. In previous studies, different composite materials and varieties of traditional manufacturing approaches were utilized for producing thin-walled composite structures [4, 8]. However, the traditional manufacturing processes such as resin transfer molding, hot-press molding, and injection molding had complex process steps and required various costly rigid molds, which hindered the wide application of thin-walled composite structures [9, 10].

Additive manufacturing (AM) offers the opportunity to easily and rapidly fabricate thin-walled composite structures with complicated cross-sectional configurations [11–13]. For instance, Wang et al. [14] investigated the effects of filling shape and filling density on the crashworthiness of 3D printed short carbon fiber reinforced thin-walled composite structures. The results showed that the circular filled structures with high filling density performed highest energy absorption. Wang et al. [15] studied 3D printed short glass and carbon fibers reinforced thin-walled structures with various cross-sectional configurations, and found that hexagonal structures made by short carbon fiber reinforced material presented the best energy absorption performance under both quasi-static compression and dynamic impact conditions. Nevertheless, the relatively poor mechanical performance of short fiber reinforced thin-walled composite structures manufactured by the 3D printing approach compared to those made by metallic materials limits their application as energy absorbing parts [16–20]. To improve the energy absorption performances of thin-walled structures prepared by composite materials, continuous fibers were beginning to be used as reinforcements introduced into 3D printing processing [21–23]. Chen et al. [24] and Ibrahim et al. [25] proposed continuous glass fibers and metal wires reinforced thin-walled composite structures with circular cross-sectional configuration through a 3D printing approach. They found that 3D printing technique could enable low-cost, customized manufacture of continuous fiber reinforced thin-walled composite structures (CFTCSs). At present, although a small number of literatures reported the feasibility of 3D printing CFTCSs, the printability and energy absorption characteristics of structures with different cross-sectional

configurations were still less reported. In addition, it is difficult for synthetic fiber reinforced non-biodegradable polymer composites to meet the requirements of environmental friendliness and sustainable development, due to the increasingly severe challenges faced by the global ecological environment. Therefore, in the development of composites thin-walled structures, environmental problems must be considered [26].

In this study, polylactic acid (PLA) and continuous ramie fibers were used as matrix and reinforcement for 3D printed environmental friendliness thin-walled structures because of their biodegradability and suitable mechanical properties [27]. The printing parameters optimization and path smoothing were conducted in order to fabricate thin-walled structures with different cross-sectional configurations conforming to the design. After that, the deformation pattern and energy absorption mechanism of the structures under quasi-static compression were investigated. Moreover, the energy absorption characteristics of structures with different cross-sectional configurations were evaluated and compared.

## 2 Materials and Methods

### 2.1 Materials and Processing

In this study, ramie yarns with a linear density of 24 Nm/2R were used (Hunan Huasheng Dongting Ramie Textile Co., Ltd, Hunan, China). Nm is the fiber's metric count and represents the length (m) of one gram of fiber at convention moisture regain. 2R means that the fiber was twisted (400 r/m) with two single strands. PLA filament with a diameter of 1.75 mm was purchased from eSUN (Shenzhen, China). Before printing, the ramie yarns were dried in an oven at 80 °C for two hours [28]. The thin-walled composite structures were fabricated by modified 3D printing equipment (Ender3 V2, Creality 3D Technology Co., Ltd., Shenzhen, China) with a single 1.3 mm diameter flat-head nozzle (Figure 1(a)). The dried ramie yarns and PLA filament were simultaneously fed into the nozzle applying the in-situ impregnation printing process.

As shown in Figure 1(b), the printed thin-walled structures with circle, hexagon and quadrangle cross-sectional configurations were designed. The circular thin-walled structure had diameter of 50 mm ( $D$ ), and the inscribed hexagonal, and quadrangular configurations had lengths of 25 mm ( $L_H$ ), and  $25\sqrt{2}$  mm ( $L_Q$ ), respectively [15]. The thickness ( $t$ ) and height ( $H$ ) of thin-walled structures were 1.9 mm and 90 mm.

The printing layer thickness and speed would affect the forming quality and deposition efficiency of continuous fibers with the matrix, which had an impact on the printing geometric accuracy of the structures, and thus on its fabrication and energy absorption characteristics [24,

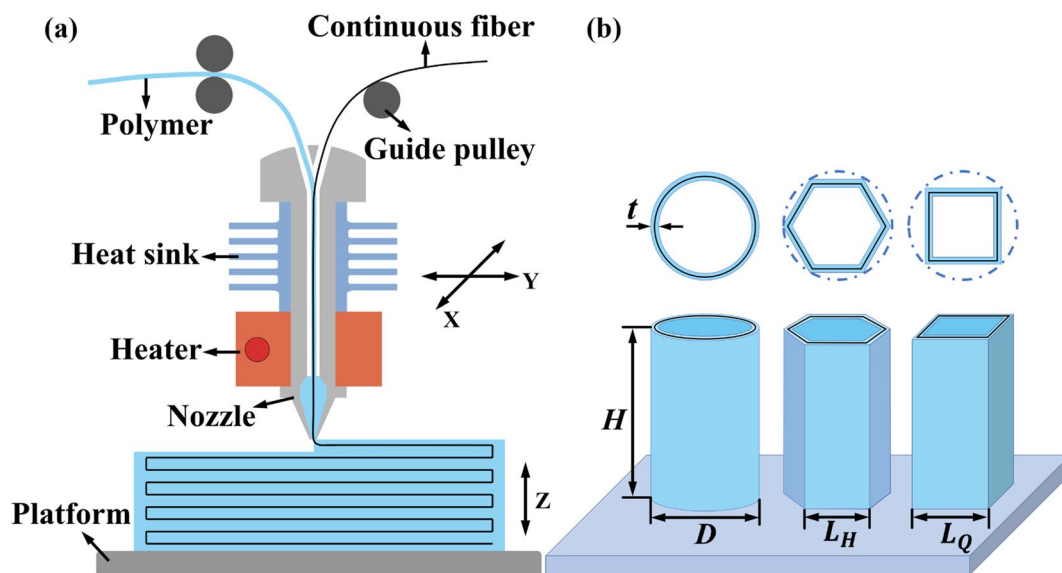


**Figure 1** Method for manufacturing the biocomposite: (a) Schematic of the 3D printing process, (b) Designed thin-walled structures

29, 30]. These two parameters were therefore selected to discuss in order to guarantee the successful manufacturing of 3D printed continuous fiber reinforced thin-walled structures.

## 2.2 Characterization

In this work, the crushing behaviors of the 3D printed thin-walled composite structures were evaluated through quasi-static compressive tests. The tests were performed on a universal mechanical testing machine (E44, MTS Co., USA), and the fixed loading rate was 10 mm/min at room temperature [31, 32]. It was noted that the corresponding load was measured within the crushing displacement of 60 mm ( $2/3 H$ ) [33, 34]. A minimum of three repeated tests were conducted on specimens of each cross-sectional shape to ensure experimental reliability. The mechanical properties of the structures presented were the average results obtained from these tests and the experimental errors were provided.

A digital camera (EOS 5D, Mark IV, Canon, Japan) was utilized to record the whole collapse process. A digital camera with capture frequency of 60 Hz was chosen for recording the deformation process of the thin-walled structures in this study. This capture frequency was chosen because it was much higher than the compressive rate (10 mm/min) of the structures. The morphological features at low magnification of the samples printed with different printing speed and layer thickness were observed by an optical microscope (AO-3M150GS, AOSVI, Shenzhen, China). In addition, the typical failure modes of the tested structures under quasi-static compression were observed with a field emission scanning

electron microscopy (SEM) (S-4800, FE-SEM, Hitachi Co., Japan).

## 3 Results and Discussions

### 3.1 Printability

#### 3.1.1 Effects of Printing Parameters

Based on the existed research on continuous fiber 3D printing of composite materials, the specimens with three configurations in this study were first prepared using the printing parameters of a single layer thickness of 0.4 mm and a printing speed of 100 mm/min [35, 36]. The corresponded cross-sectional surfaces of the three structures are shown in Figure 2. In this study, the geometric accuracy of the printed specimens was used to evaluate the printability. It could be found in Figure 2 that the printed specimens with circular and hexagonal configurations presented relatively good shape accuracy. More specifically, low deviations between designed and printed paths for the continuous fiber were observed for the structures with circular and hexagonal shapes compared with the specimen with quadrangular configuration (as shown in Figure 2(a), (b)). These deviations were more significant at the corner area for the specimen with quadrangular configuration as shown in Figure 2(c). In this figure, the deposited continuous fiber strands presented a large offset toward the inner side of the specimens at the  $90^\circ$  corner position, resulting in an adverse effect on the printing quality of the printed structures. Many studies had illustrated that when printing polymer parts filled with continuous fiber, the shape precision was usually poor at corner regions, especially at sharp curvatures [37–39]. In addition, it was well known that the printing quality of

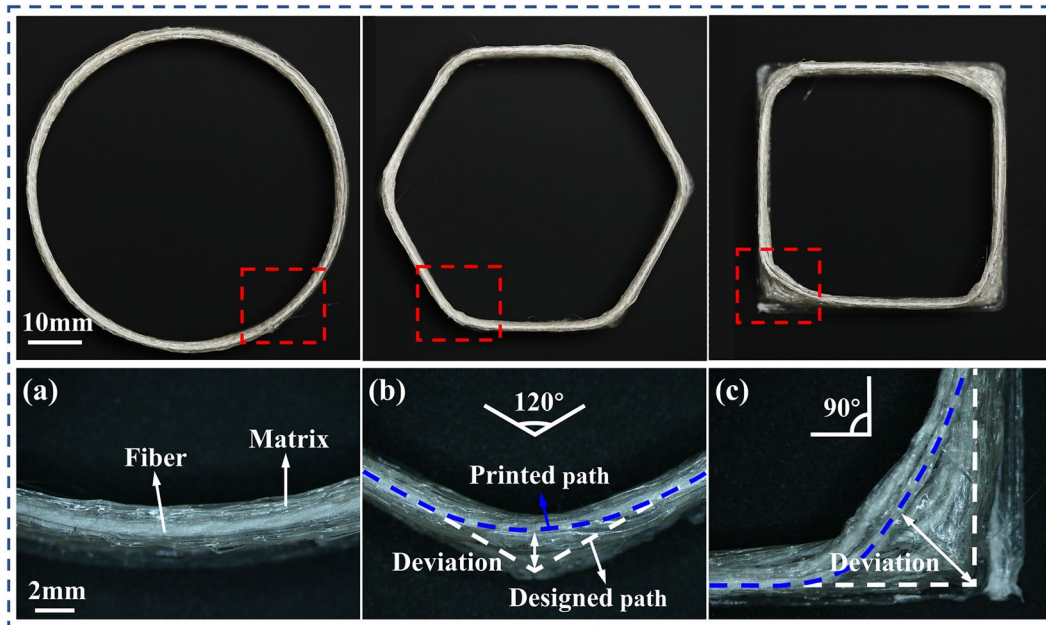


**Figure 2** Cross-sectional images of specimens with different shapes under a printing speed of 100 mm/min and a layer thickness of 0.4 mm

the 3D printed components was significantly affected by printing parameters [40–42]. Therefore, this study tried to adjust the printing parameters to obtain the printed specimens with the better printing geometric accuracy. Among the three shapes of specimens in this study, the rectangular specimen was selected as the objective to obtain appropriate printing parameters because it had higher curvature compared with specimens of other shapes and accordingly showed the larger geometric deviations as discussed above.

Figure 3 shows rectangular specimens printed under different printing speeds and layer thicknesses, which were two key printing parameters influencing the printing quality. The tags F100 and L0.2 meant printed specimens prepared with a printing speed of 100 mm/min and a layer thickness of 0.3 mm, and other tags had the similar meaning. In this figure, it could be seen that at higher printing speeds (300 and 500 mm/min), the specimens presented poorer printing geometric accuracy (as shown in Figure 3(d)–(i)), with higher deviations between designed and printed paths. During the in-situ impregnation printing process, the matrix was extruded in a semi-molten state and the fibers stuck in the matrix were dragged and deposited with the matrix as the nozzle moved. During the printing process, the extruded semi-molten matrix did not hold the fibers well, so when the dragging force of the nozzle was high, the fibers were pulled out from the matrix. When printing sharp corners, the nozzle would decelerate and accelerate inevitably, leading to a non-uniform

dragging force [43]. Especially, at a high printing speed, the velocity change of the nozzle and corresponding dragging force will be very high at the sharp corners. As a result, at high printing speeds, the fibers were easier to be pulled out from matrix when printing sharp corners. In addition, as the printing speed increased, the deposited material had less time to cool and solidify, which means that the matrix had less binding force on the fiber, resulting in the fiber being more easily pulled out from the matrix.

In addition, at high printing speeds (300 and 500 mm/min), printing geometric accuracy deteriorated with the increase of layer thicknesses. However, when the printing speed was low (100 mm/min), it seemed that shape accuracy of specimen printed at layer thickness of 0.25 mm (see Figure 4(b)) was superior to that at layer thickness of 0.2 mm (see Figure 4(a)). The layer thickness could affect the contact pressure between the material being extruded from the nozzle and the deposited material [24, 44, 45]. Lower layer thickness caused a tight space for depositing and a higher contact pressure between layers, leading to a better bonding of matrix and fibers as reported in Refs. [24, 28, 44]. Therefore, at low layer thickness, the fiber was not easily to be pulled out from the matrix. However, when the layer thickness was low and the printing speed was slow, the nozzle pressure would be high, pushing the matrix to both sides of the deposition path, and consequently resulting in reduced constraints of the matrix for the fiber, as well as matrix-rich region in the corner,

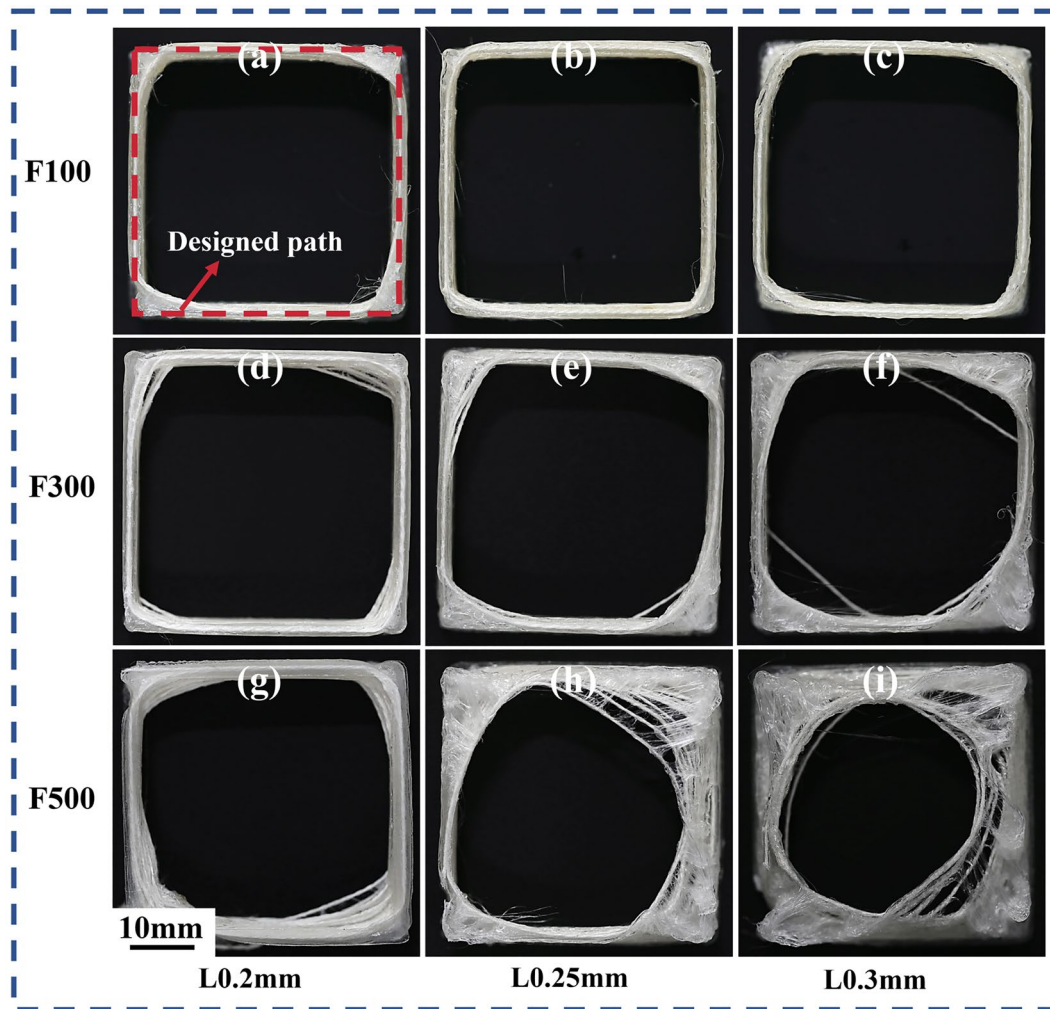


**Figure 3** Crosse-sectional images for printed rectangular structures with different combinations of printing speed and layer thickness

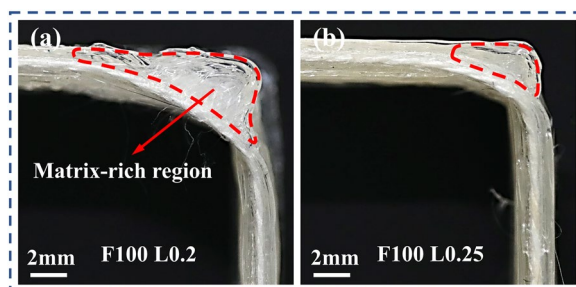


**Figure 4** Images of the printed specimen with quadrangular configuration at the 90° corner position under a printing speed of 100 mm/min

as shown in Figure 4(a). Therefore, low layer thickness could also make the printing geometric accuracy at sharp corners worse.

### 3.1.2 Corners Path Smoothing

It was found that after printing parameters optimization, the quadrangular tubes still presented the problem that the continuous fiber was not deposited according to the design path, as illustrated in Figure 4(b). Therefore, the printing geometric accuracy of thin-walled structure with quadrangular configuration still needed to be improved. In addition to varying printing parameters, Refs. [46, 47] found that shape accuracy could also be improved by adjusting the print path at the corners when printing pure matrix. These works indicated that when printing sharp corners, path smoothing could improve the printing accuracy at corners. Therefore, this study attempted to make path smoothing in rounding off the corners with different radii ( $R$ ) by modifying the  $G$ -code. The rectangular specimens with rounded corners of different radii printed at a printing speed of 100 mm/min and a layer thickness of 0.25 mm are shown in

Figure 5. The distance ( $\delta$ ) between the corner bisector of the designed right-angle corner and the actual deposited continuous fiber was used to quantify the printing geometric accuracy at the corner, as illustrated in Figure 5(a). The  $\delta$  for printed specimens with rounded corners of different radii is presented in Figure 5(e). In this study, the radii of rounded corners were set to  $R = 1$  mm,  $R = 2$  mm and  $R = 3$  mm. It could be found in this figure that compared with the specimens without amended rounded corners, the  $\delta$  of the specimens with  $R = 1$  mm and  $R = 2$  mm were reduced by 39.9% and 10.7%, respectively. However, when  $R$  continued to raise to 3 mm, the value of  $\delta$  was larger than that of the unrounded corner. As discussed above, the inevitable velocity changes of nozzle movement when printing sharp corners could lead to deviations between the actual fiber path and the designed fiber path. Rounding the sharp corners of the structure through path design and using rounded corners with the appropriate radius could mitigate this influence, thus improving deposition quality at the corners. Rounded corners with too large radius made the printed path too far from the desired right-angle path and did not achieve the desired shape. According to the above results, after printing parameters and printing path optimization, continuous ramie fiber filled thin-walled structures with circular, hexagonal, and quadrangular configurations were printed at a printing speed of 100 mm/min and a layer

thickness of 0.25 mm. The thin-walled structures were successfully manufactured.

### 3.2 Quasi-Static Compression Responses

#### 3.2.1 Collapse Modes

Figure 6 presents the deformation and collapse processes of thin-walled structures with three shapes under quasi-static compression. In this figure, it was found that thin-walled structures gradually collapsed under quasi-static compression loading. Specifically, the wall of the structure began to plastic deformation, buckle or break locally after the initial elastic stage, forming a folding wrinkle. As the compression continued, the folded part was compacted, and the next similar folding wrinkle began to form until the structure was completely compacted. Thin-walled structures with three shapes showed similar progressive deformation patterns but had some differences. For structure with circular configuration, the first folding wrinkle was formed by buckling near the upper plate, and there was no obvious second folding wrinkle before compaction. For structure with hexagonal shape, the first folding wrinkle was also near the upper plate formed by buckling, but as the compression continued, it was found that the second folding wrinkle was formed below the first folding. As for structure with quadrangular configuration, unlike the former two shapes structures, the first folding wrinkle appeared in the middle of

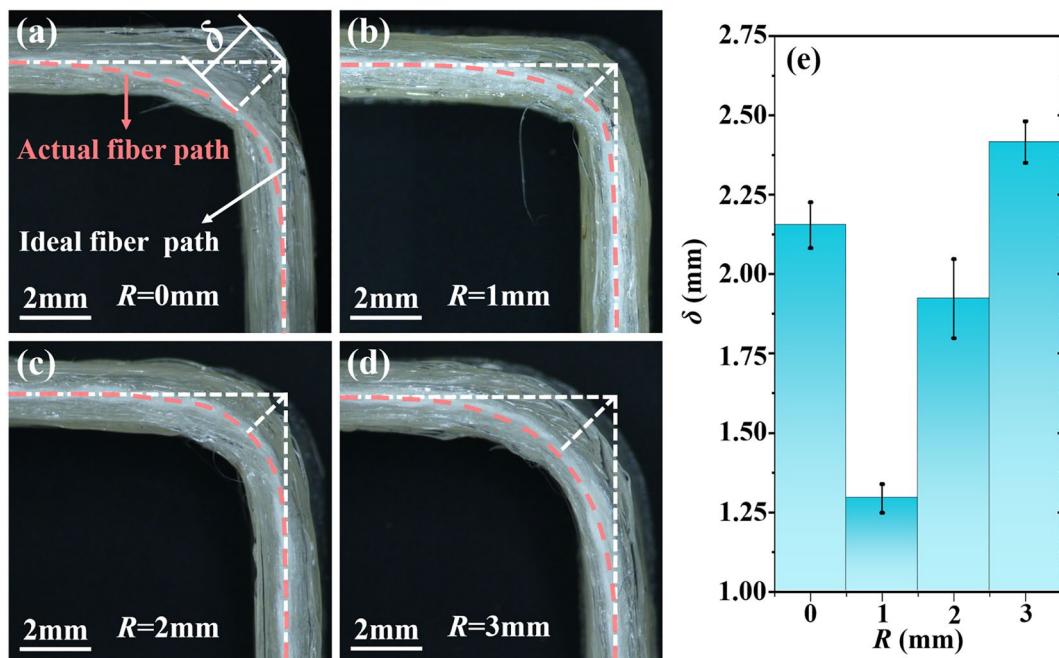


**Figure 5** Images of printed rectangular specimens with rounded corners of different radii ( $R$ ): (a)  $R = 0$  mm, (b)  $R = 1$  mm, (c)  $R = 2$  mm, (d)  $R = 3$  mm, (e) Distance ( $\delta$ ) between the actual deposited continuous fiber and the corner bisector of the designed right-angle corner

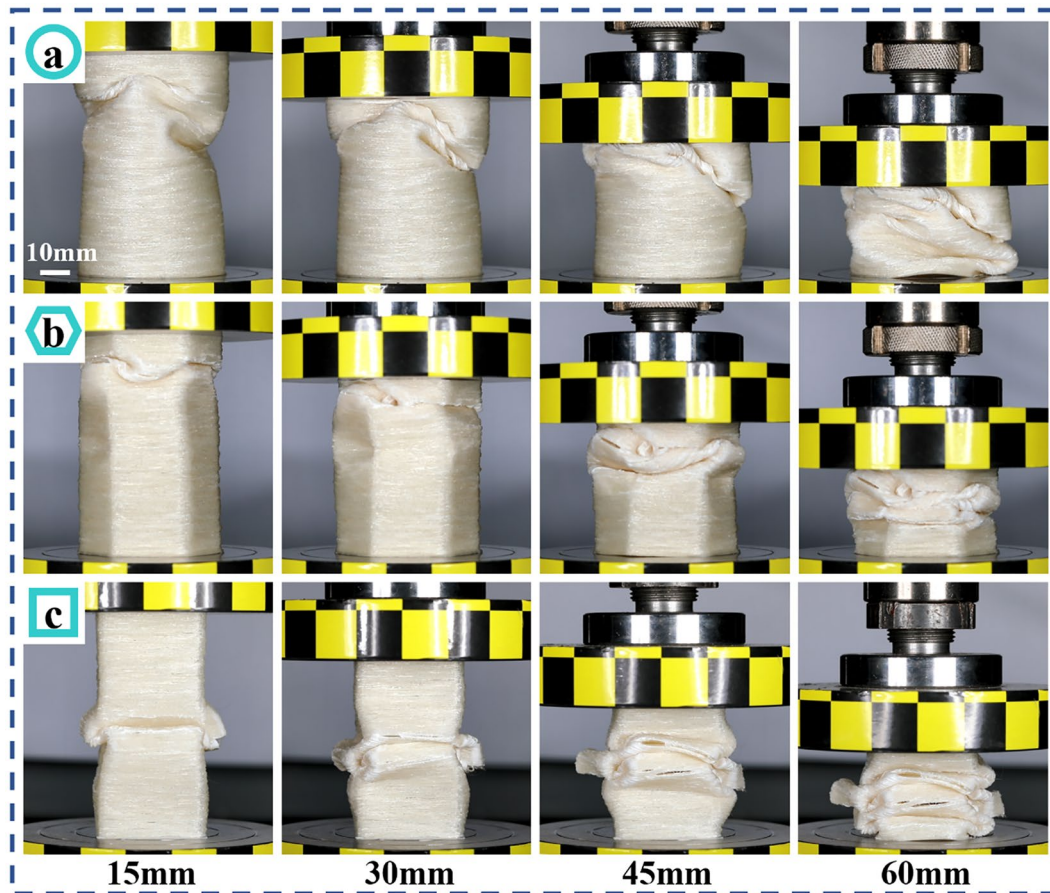


**Figure 6** Quasi-static collapse modes of 3D printed thin-walled structures with (a) circle, (b) hexagon and (c) quadrangular configurations

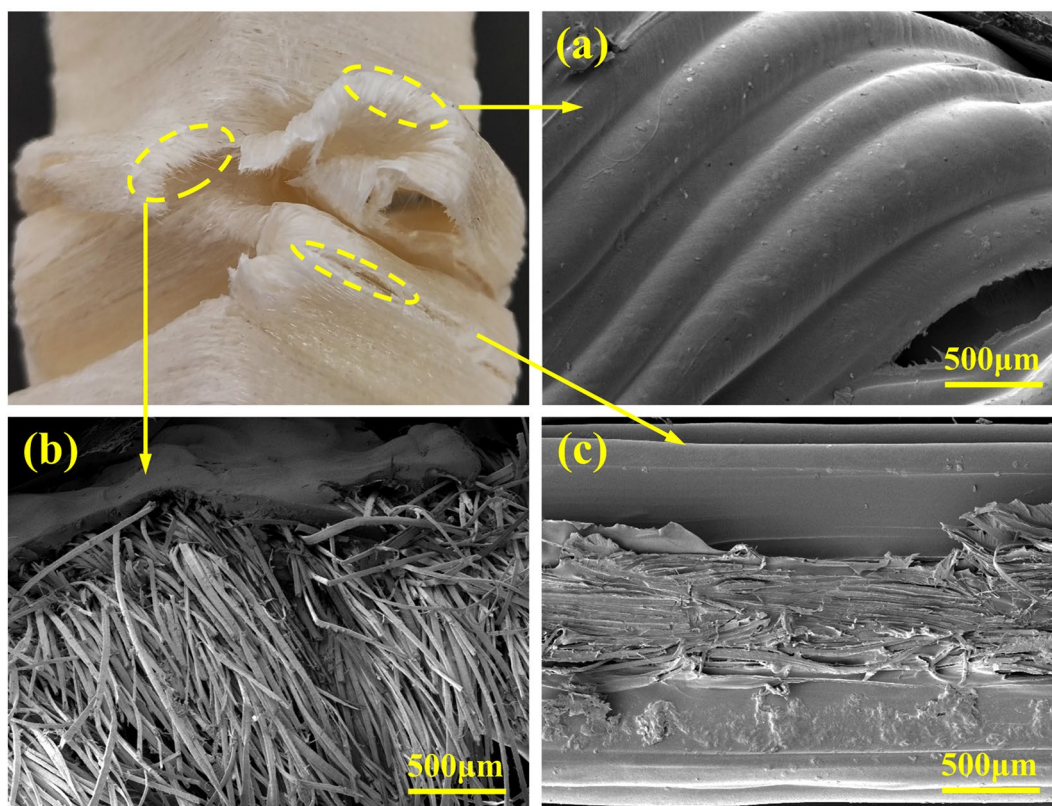
the tube, and the distinct rupture of wall could be seen in Ref. [15].

Figure 7 shows the typical failure modes of the structures under quasi-static compression. In this figure, three typical failure modes could be seen: (a) Local buckling deformation and matrix cracking when local deformation was large, as shown in Figure 7(a); (b) fracture along the vertical axial direction of the tube wall and ramie fibers were pulled out from matrix and were fractured, as shown in Figure 7(b); (c) delamination along the horizontal direction of the structure wall (including matrix/matrix debonding and matrix/fiber debonding, as shown in Figure 7(c)). Large local buckling deformation was a common failure mode for thin-walled structures [48–50]. Specifically, the printed structures absorbed energy through plastic deformation together with cracks and fractures during the quasi-static compression process. The thin-walled structures in this study were fabricated by in-situ impregnation fused deposition modeling

technique, so relatively poor adhesion between layers might be one possible reason of fracture along the horizontal direction of the structure wall [44]. Such delamination could affect the load bearing capacity of the structure, as the composite layers affected by this phenomenon lose their capability to effectively distribute stresses. In addition, the layered cracking could prevent the excessive plastic bending required for the folding process (as in the structure with circular configuration) [51].

### 3.2.2 Force-Displacement Responses

To investigate the mechanical performance of 3D printed continuous ramie fiber reinforced thin-walled structures with three shapes, representative force-displacement curves for three different structures are shown in Figure 8. Additionally, to better evaluate the variation on the mechanical performance of the tested samples, the force-displacement curves of thin-walled structures with the same cross-sectional shape are



**Figure 7** SEM micrographs of typical failure modes of the structures under compression: (a) Local buckling deformation, (b) Fiber pullout, (c) Delamination

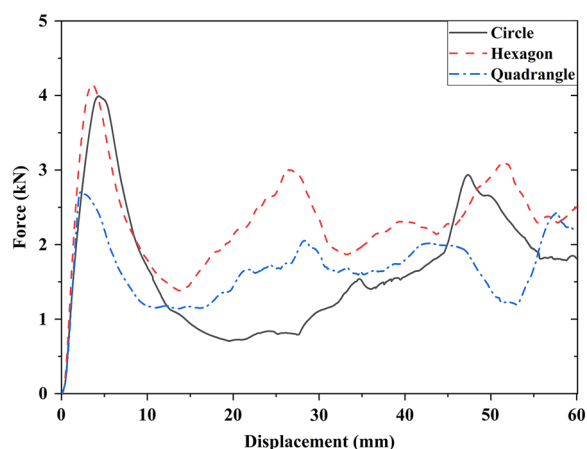


**Figure 8** Force-displacement curves of thin-walled structures with circle, hexagon and quadrangular configurations

shown in Figure 9. It was found in Figure 8 that thin-walled structures with quadrangular configuration

required smaller forces to initiate the crushing compared to the other structures. Moreover, it was found that all the force first rose rapidly to reach the first wrinkle, which corresponded to the forming of the first wrinkle. Thereafter, the force-displacement curves declined to the first trough, indicating that the first wrinkle was compacted. Next, the curves continued to fluctuate, corresponding to the progressive folding process of the structures. The number of waves in the curves of thin-walled structures was in good agreement with the corresponded deformation and collapse processes as discussed in Figure 6. Specifically, the force-displacement curve for circular structure showed fewer waves than those of other structures, corresponding to the fewer formed compression folds of circular structure during compression as shown in Figure 6a. Due to the mix of different failure behaviors for energy dissipating, such as delamination, fiber breakage and matrix cracking, the force-displacement curves showed a few irregular sharp peaks.



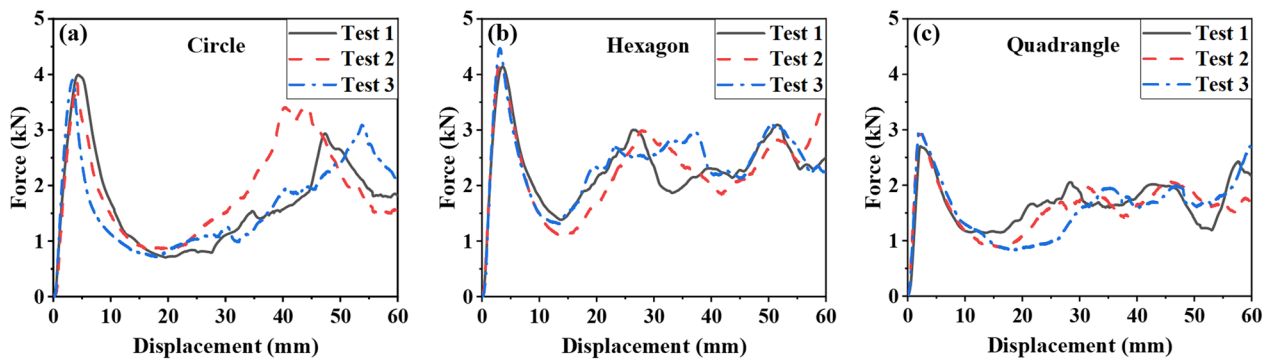


**Figure 9** Force-displacement curves for repeatability tests of thin-walled structures with (a) circle, (b) hexagon and (c) quadrangular configurations

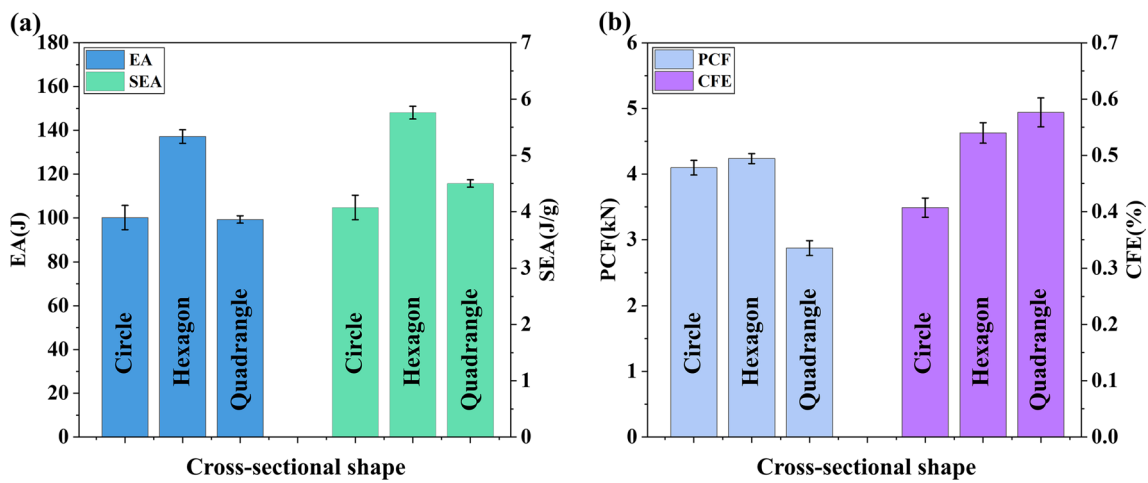


**Figure 10** Energy absorption characteristics: (a) EA and SEA, (b) PCF and CFE, of thin-walled structures with circle, hexagon and quadrangular shapes

### 3.3 Energy Absorption Performance

Based on the force-displacement curves, the key indicators for evaluating the energy absorption performance of the thin-walled structures were calculated, as shown in Figure 10 [52]. Notably, the mechanical properties of each test specimen were calculated based on their respective measured geometries. In this study, energy absorbed (EA) by the structure was calculated as the area enclosed by the force-displacement curve, as shown in Eq. (1):

$$EA = \int_0^d F(x)dx, \tag{1}$$

where  $F(x)$  is the force at displacement  $x$ , and  $d$  is the total displacement.

For comparing different structures considering mass differences, specific energy absorption (SEA) was

computed based on energy absorbed per unit mass ( $m$ ), as described in Eq. (2):

$$SEA = \frac{EA}{m}. \tag{2}$$

A greater SEA meant higher potential for lightweight applications of the structure.

In addition to the metrics for energy absorption capability, some other characteristics in the compression process could also reflect the energy absorption performance of the structure, such as peak crush force (PCF), mean crush force (MCF), as well as crush force efficiency (CFE). PCF was generally expected to be a relatively low value to ensure safety during energy absorption process [51]. MCF represented the average crushing force in the crushing process, as expressed in Eq. (3):

$$MCF = \frac{\int_0^d F(x)dx}{d}. \quad (3)$$

CFE was used to evaluate the uniformity of the crushing force. And it could be obtained based on the PCF and MCF, as presented in Eq. (4):

$$CFE = \frac{MCF}{PCF}. \quad (4)$$

Usually, CFE was expected to be a relatively high value. In conclusion, it was considered that a good energy absorber should have high SEA and CFE but low PCF [53–56].

In Figure 10, it can be seen that the thin-walled structures with circular shape showed lower SEA and CFE as well as higher PCF than those of other structures, suggesting that circular thin-walled structures had an inferior energy absorption performance than structures with other configurations in this study. This was related to that the circular thin-walled structure formed fewer wrinkles as exhibited above. Wang et al. [15] reported that more wrinkles with shorter wavelengths were salutary to the energy absorption during the progressive collapse process of the thin-walled structures. Compared with quadrangular configuration, the thin-walled structures with hexagonal configuration presented higher SEA. It seemed that the deformation and collapse mode of the thin-walled structure with hexagonal configuration was more ideally conducive to energy absorption. Although the EA and SEA of the square configuration were lower than that of the hexagonal configuration, it had lower PCF, which was beneficial in some energy absorption applications that paid more attention to safety protection.

Comparing the SEA and CFE of thin-walled structures in this study and those of other thin-walled structures reported in literature under quasi-static compression, it was found that 3D printed continuous ramie fiber reinforced thin-walled structures could present similar even higher CFE and SEA than other structures, indicating their great potential for energy absorber application [15, 57]. Note that most of the thin-walled structures in the literature were made of metals, non-biodegradable plastics and short fiber reinforced composites. In contrast, the thin-walled structures in this study were fabricated by biodegradable PLA and natural ramie fiber. Therefore, 3D printed continuous ramie fiber reinforced thin-walled structures have the promising potential to apply for energy absorber while meeting the requirements of environmental friendliness and sustainability.

## 4 Conclusions

In this study, continuous ramie fiber reinforced thin-walled structures with good geometric accuracy were successfully fabricated by in-situ impregnation 3D printing technique through parameter optimization and path smoothing. In addition, the failure behavior and energy absorption characteristics of the structures with different section shapes under quasi-static axial loading conditions were investigated. Based on the experimental results, the conclusions are summarized as follows:

- (1) The 3D printed continuous fiber reinforced thin-walled structures with quadrilateral configurations fabricated at a printing speed of 100 mm/min and a layer thickness of 0.25 mm exhibited the best geometric accuracy. Printing defects at the corners of specimens increased as the printing speed increased, and too low layer thicknesses reduced the geometric accuracy at the corners.
- (2) Shape accuracy at corners could be further improved by optimizing the printing path. The rounded corners with appropriate radius presented better printing geometric accuracy compared with those without rounding.
- (3) For all the thin-walled structures in this study, a progressive deformation pattern was exhibited during quasi-static compression.
- (4) Energy absorption of the structures was implemented through the combined damage modes of plastic deformation, fiber pullout and delamination.
- (5) The hexagonal structure exhibited the highest SEA. The square structure showed lower energy absorption than the hexagonal structure, but higher CFE.

This study demonstrated that continuous ramie fiber reinforced simple thin-walled structures have great potential when used in energy absorbing devices. In future works, the energy absorption properties could be further enhanced by designing 3D printed multi-cell filled thin-walled structures.

### Acknowledgements

Not applicable.

### Authors' Contributions

KW and HZ were in charge of the whole trial; HL wrote the manuscript; RC assisted with sampling and laboratory analyses; AL and PC discussed the structure of the paper. YH and YP reviewed and edited the manuscript. All authors read and approved the final manuscript.

### Authors' information

Kui Wang, born in 1984, is currently a professor and a PhD candidate supervisor at *School of Traffic & Transportation Engineering, Central South University, China*. His research interests include integrated design and manufacture of material structure and function.

Hao Lin, born in 1999, is currently a master candidate at *Central South University, China*.

Antoine Le Duigou, born in 1983, is currently an associate professor at *University of South Brittany, France*. His research interests include bioinspired shapechanging materials and structures.

Ruijun Cai, born in 1997, is currently a master candidate at *Central South University, China*.

Yangyu Huang, born in 2001, is currently a doctoral candidate at *Central South University, China*.

Ping Cheng, born in 1992, is currently a doctoral candidate at *Central South University, China*.

Honghao Zhang, born in 1992, is currently a lecturer at *Shandong University, China*. His research interests include safety engineering and green manufacturing.

Yong Peng, born in 1984, is currently a professor and a PhD candidate supervisor at *School of Traffic & Transportation Engineering, Central South University, China*. His research interests include vehicle safety and accident analysis.

### Funding

Supported by National Natural Science Foundation of China (Grant Nos. 51905555, 52105523), Hu-Xiang Youth Talent Program of China (Grant No. 2020RC3009), and Innovation-Driven Project of Central South University of China (Grant No. 2019CX017).

### Data availability

Data will be made available on reasonable request.

### Declarations

#### Competing Interests

The authors declare no competing financial interests.

#### Author Details

<sup>1</sup>Key Laboratory of Traffic Safety on Track of Ministry of Education, School of Traffic and Transportation Engineering, Central South University, Changsha 410075, China. <sup>2</sup>Institute de Research Dupuy de Lôme, Bionics Group, University of South Brittany, Lorient F-56100, France. <sup>3</sup>ICUBE Laboratory-CNRS, University of Strasbourg, Strasbourg 67000, France. <sup>4</sup>Key Laboratory of High Efficiency and Clean Mechanical Manufacture (Ministry of Education), School of Mechanical Engineering, Shandong University, Jinan 250061, China.

Received: 29 October 2022 Revised: 10 November 2023 Accepted: 14 November 2023

Published online: 12 December 2023

### References

- [1] G W Zhou, Q P Sun, J Fenner, et al. Crushing behaviors of unidirectional carbon fiber reinforced plastic composites under dynamic bending and axial crushing loading. *International Journal of Impact Engineering*, 2020, 140: 103539.
- [2] P Cheng, Y Peng, K Wang, et al. Study on intralaminar crack propagation mechanisms in single-and multi-layer 2D woven composite laminate. *Mechanics of Advanced Materials and Structures*, 2021: 1-11.
- [3] P Cheng, Y Peng, K Wang, et al. Mechanical performance and damage behavior of delaminated composite laminates subject to different modes of loading. *Journal of the Brazilian Society of Mechanical Sciences and Engineering*, 2021, 43(10): 1-10.
- [4] M Rogala, J Gajewski, K Gawdzinska. Crashworthiness analysis of thin-walled aluminum columns filled with aluminum-silicon carbide composite foam. *Composite Structures*, 2022, 299: 116102.
- [5] M A Abd El-baky, D A Hegazy, M A Hassan. Advanced thin-walled composite structures for energy absorption applications. *Applied Composite Materials*, 2022, 29(3): 1195-1233.
- [6] C W Isaac, C Ezekwem. A review of the crashworthiness performance of energy absorbing composite structure within the context of materials, manufacturing and maintenance for sustainability. *Composite Structures*, 2021, 257: 113081.
- [7] Y S Liu, J Wang, R J Cai, et al. Effects of loading rate and temperature on crushing behaviors of 3D printed multi-cell composite tubes. *Thin-Walled Structures*, 2023, 182: 110311.
- [8] P Rozylo. Failure analysis of thin-walled composite structures using independent advanced damage models. *Composite Structures*, 2021, 262: 113598.
- [9] J M Chacon, M A Caminero, P J Nunez, et al. Additive manufacturing of continuous fibre reinforced thermoplastic composites using fused deposition modelling: Effect of process parameters on mechanical properties. *Composites Science and Technology*, 2019, 181: 107688.
- [10] F Quadrini, E A Squeo. Injection molding of bushes made of tribological PEEK composites. *Express Polymer Letters*, 2007, 1(12): 817-823.
- [11] S E Alkhatib, M S Matar, F Tarlochan, et al. Deformation modes and crashworthiness energy absorption of sinusoidally corrugated tubes manufactured by direct metal laser sintering. *Engineering Structures*, 2019, 201: 109838.
- [12] A S Mohamed, O Laban, F Tarlochan, et al. Experimental analysis of additively manufactured thin-walled heat-treated circular tubes with slits using AlSi10Mg alloy by quasi-static axial crushing test. *Thin-Walled Structures*, 2019, 138: 404-414.
- [13] P Cheng, Y Peng, K Wang, et al. Quasi-static penetration property of 3D printed woven-like ramie fiber reinforced biocomposites. *Composite Structures*, 2023, 303: 116313.
- [14] K Wang, Y S Liu, J Wang, et al. On crashworthiness behaviors of 3D printed multi-cell filled thin-walled structures. *Engineering Structures*, 2022, 254: 113907.
- [15] J Wang, Y S Liu, K Wang, et al. Progressive collapse behaviors and mechanisms of 3D printed thin-walled composite structures under multi-conditional loading. *Thin-Walled Structures*, 2022, 171: 108810.
- [16] H Al Abadi, H T Thai, V Paton-Cole, et al. Elastic properties of 3D printed fibre-reinforced structures. *Composite Structures*, 2018, 193: 8-18.
- [17] U Morales, A Esnaola, M Iragi, et al. Quasi-static and dynamic crush behaviour of 3D printed thin-walled profiles reinforced with continuous carbon and glass fibres. *Composites Part B: Engineering*, 2021, 217: 108865.
- [18] A Le Duigou, D Correa, M Ueda, et al. A review of 3D and 4D printing of natural fibre biocomposites. *Materials & Design*, 2020, 194: 108911.
- [19] V T Le, T Jin, N S Goo. Mechanical behaviors and fracture mechanisms of CFRP sandwich composite structures with bio-inspired thin-walled corrugated cores. *Aerospace Science and Technology*, 2022, 126: 107599.
- [20] K Wang, Y Lu, Y N Rao, et al. New insights into the synergistic influence of voids and interphase characteristics on effective properties of unidirectional composites. *Composite Structures*, 2021, 255: 112862.
- [21] X J Chen, G X Fang, W H Liao, et al. Field-based toolpath generation for 3D printing continuous fibre reinforced thermoplastic composites. *Additive Manufacturing*, 2022, 49: 102470.
- [22] H Mei, Z S Ali, I Ali, et al. Tailoring strength and modulus by 3D printing different continuous fibers and filled structures into composites. *Advanced Composites and Hybrid Materials*, 2019, 2: 312-319.
- [23] P Cheng, Y Peng, S X Li, et al. 3D printed continuous fiber reinforced composite lightweight structures: A review and outlook. *Composites Part B: Engineering*, 2022: 110450.
- [24] K Chen, L G Yu, Y H Cui, et al. Optimization of printing parameters of 3D-printed continuous glass fiber reinforced polylactic acid composites. *Thin-Walled Structures*, 2021, 164: 107717.
- [25] Y Ibrahim, G W Melenka, R Kempers. Additive manufacturing of continuous wire polymer composites. *Manufacturing Letters*, 2018, 16: 49-51.
- [26] B C Mitra. Environment friendly composite materials: Biocomposites and Green composites. *Defence Science Journal*, 2014, 64(3): 244-261.
- [27] C Baley, M Gomina, J Breard, et al. Variability of mechanical properties of flax fibres for composite reinforcement: A review. *Industrial Crops and Products*, 2020, 145: 111984.
- [28] P Cheng, K Wang, X Z Chen, et al. Interfacial and mechanical properties of continuous ramie fiber reinforced biocomposites fabricated by in-situ impregnated 3D printing. *Industrial Crops and Products*, 2021, 170: 113760.
- [29] A Le Duigou, M Castro, R Bevan, et al. 3D printing of wood fibre biocomposites: From mechanical to actuation functionality. *Materials & Design*, 2016, 96: 106-114.

- [30] S M F Kabir, K Mathur, A F M Seyam. A critical review on 3D printed continuous fiber-reinforced composites: History, mechanism, materials and properties. *Composite Structures*, 2020, 232: 111476.
- [31] X Liu, B Belkassam, A Jonet, et al. Experimental investigation of energy absorption behaviour of circular carbon/epoxy composite tubes under quasi-static and dynamic crush loading. *Composite Structures*, 2019, 227: 111266.
- [32] N Movahedi, E Linul. Quasi-static compressive behavior of the ex-situ aluminum-alloy foam-filled tubes under elevated temperature conditions. *Materials Letters*, 2017, 206: 182-184.
- [33] G Y Sun, S F Li, Q Liu, et al. Experimental study on crashworthiness of empty/aluminum foam/honeycomb-filled CFRP tubes. *Composite Structures*, 2016, 152: 969-993.
- [34] N Qiu, Y K Gao, J G Fang, et al. Theoretical prediction and optimization of multi-cell hexagonal tubes under axial crushing. *Thin-Walled Structures*, 2016, 102: 111-121.
- [35] C J Zeng, L W Liu, W F Bian, et al. Compression behavior and energy absorption of 3D printed continuous fiber reinforced composite honeycomb structures with shape memory effects. *Additive Manufacturing*, 2021, 38: 101842.
- [36] C J Zeng, L W Liu, W F Bian, et al. Bending performance and failure behavior of 3D printed continuous fiber reinforced composite corrugated sandwich structures with shape memory capability. *Composite Structures*, 2021, 262: 113626.
- [37] R Matsuzaki, T Nakamura, K Sugiyama, et al. Effects of set curvature and fiber bundle size on the printed radius of curvature by a continuous carbon fiber composite 3D printer. *Additive Manufacturing*, 2018, 24: 93-102.
- [38] C Quan, B Han, Z H Hou, et al. 3D printed continuous fiber reinforced composite auxetic honeycomb structures. *Composites Part B: Engineering*, 2020, 187: 107858.
- [39] T Fruleux, M Castro, D Correa, et al. Geometric limitations of 3D printed continuous flax-fiber reinforced biocomposites cellular lattice structures. *Composites Part C: Open Access*, 2022, 9: 100313.
- [40] Z H Hou, X Y Tian, J K Zhang, et al. 3D printed continuous fibre reinforced composite corrugated structure. *Composite Structures*, 2018, 184: 1005-1010.
- [41] R J Cai, K Wang, W Wen, et al. Application of machine learning methods on dynamic strength analysis for additive manufactured polypropylene-based composites. *Polymer Testing*, 2022, 110: 107580.
- [42] A Le Duigou, G Chabaud, R Matsuzaki, et al. Tailoring the mechanical properties of 3D-printed continuous flax/PLA biocomposites by controlling the slicing parameters. *Composites Part B: Engineering*, 2020, 203: 108474.
- [43] Y A Jin, Y He, J Z Fu, et al. Optimization of tool-path generation for material extrusion-based additive manufacturing technology. *Additive Manufacturing*, 2014, 1: 32-47.
- [44] R J Cai, W Wen, K Wang, et al. Tailoring interfacial properties of 3D-printed continuous natural fiber reinforced polypropylene composites through parameter optimization using machine learning methods. *Materials Today Communications*, 2022, 32: 103985.
- [45] R J Cai, H Lin, P Cheng, et al. Investigation on dynamic strength of 3D-printed continuous ramie fiber reinforced biocomposites at various strain rates using machine learning methods. *Polymer Composites*, 2022, 43(8): 5235-5249.
- [46] R Comminal, M P Serdeczny, D B Pedersen, et al. Motion planning and numerical simulation of material deposition at corners in extrusion additive manufacturing. *Additive Manufacturing*, 2019, 29: 100753.
- [47] H Giberti, L Sbaglia, M Urgo. A path planning algorithm for industrial processes under velocity constraints with an application to additive manufacturing. *Journal of Manufacturing Systems*, 2017, 43: 160-167.
- [48] H L Mou, J Xie, J Zou, et al. Experimental researches on failure and energy absorption of composite laminated thin-walled structures. *Journal of Composite Materials*, 2020, 54(27): 4253-4268.
- [49] S Pirmohammad, S E Marzdashti. Crushing behavior of new designed multi-cell members subjected to axial and oblique quasi-static loads. *Thin-Walled Structures*, 2016, 108: 291-304.
- [50] G H Zhu, Q Yu, X Zhao, et al. Energy-absorbing mechanisms and crashworthiness design of CFRP multi-cell structures. *Composite Structures*, 2020, 233: 111631.
- [51] A Baroutaji, A Arjunan, G Singh, et al. Crushing and energy absorption properties of additively manufactured concave thin-walled tubes. *Results in Engineering*, 2022, 14: 100424.
- [52] N S Ha, G X Lu. Thin-walled corrugated structures: A review of crashworthiness designs and energy absorption characteristics. *Thin-Walled Structures*, 2020, 157: 106995.
- [53] T T Chen, Y Zhang, J M Lin, et al. Theoretical analysis and crashworthiness optimization of hybrid multi-cell structures. *Thin-Walled Structures*, 2019, 142: 116-131.
- [54] Y F Chen, Z H Bai, L W Zhang, et al. Crashworthiness analysis of octagonal multi-cell tube with functionally graded thickness under multiple loading angles. *Thin-Walled Structures*, 2017, 110: 133-139.
- [55] M A Rad, A Khalkhali. Crashworthiness multi-objective optimization of the thin-walled tubes under probabilistic 3D oblique load. *Materials & Design*, 2018, 156: 538-557.
- [56] H Nikkhah, A Baroutaji, Z Kazanci, et al. Evaluation of crushing and energy absorption characteristics of bio-inspired nested structures. *Thin-Walled Structures*, 2020, 148: 106615.
- [57] A A Nia, M Parsapour. Comparative analysis of energy absorption capacity of simple and multi-cell thin-walled tubes with triangular, square, hexagonal and octagonal sections. *Thin-Walled Structures*, 2014, 74: 155-165.

**Submit your manuscript to a SpringerOpen® journal and benefit from:**

- Convenient online submission
- Rigorous peer review
- Open access: articles freely available online
- High visibility within the field
- Retaining the copyright to your article

---

Submit your next manuscript at ► [springeropen.com](https://www.springeropen.com)

---